Nanoscale

Accepted Manuscript

This article can be cited before page numbers have been issued, to do this please use: M. Li, Y. Lao, R. L. Mintz, Z. Chen, D. Shao, H. Hu, H. Wang, Y. Tao and K. Leong, *Nanoscale*, 2019, DOI: 10.1039/C8NR08337A.

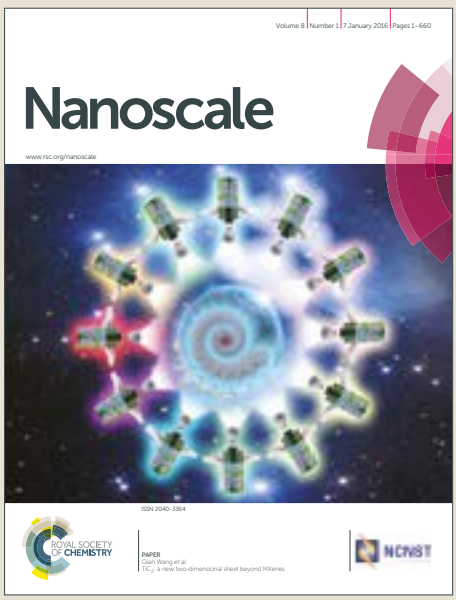

ROYAL SOCIETY OF CHEMISTRY

rsc.li/nanoscale

View Article Online
DOI: 10.1039/C8NR08337A

Nanoscale

COMMUNICATION

Multifunctional mesoporous silica-gold nanocluster hybrid platform for selective breast cancer cell detection using catalytic amplification–based colorimetric assay

Received 00th January 20xx,
Accepted 00th January 20xx

DOI: 10.1039/x0xx00000x

www.rsc.org/

Mingqiang Li,[a,b] Yeh-Hsing Lao,[b] Rachel L. Mintz,[b] Zhuanggui Chen,[a] Dan Shao,[b] Hanze Hu,[b] Hongxia Wang,[b] Yu Tao*[a,c] and Kam W. Leong*[b,d]

Breast cancer is the most common malignancy and also the second leading cause of cancer mortality in women globally. Strategies for early and precise detection of breast cancer cells are highly desired in breast cancer diagnosis and treatment. Here, we report on an efficient detection of HER2-positive (HER2$^+$) breast cancer cells using an amplified signal scheme enabled by gold nanoclusters entrapped in mesoporous silica nanoparticles (MSN). The utilization of MSN as an excellent enzyme immobilization support and gold nanoclusters as an effective peroxidase mimic imparts high sensitivity to this detection platform. In addition, the inclusion of target-specific HER2 antibodies adds excellent selectivity. Determination of HER2$^+$ cancer cells in breast cancer tissue demonstrates the potential application of this biosensor design in clinical diagnosis in particular, and bioanalysis in general.

Breast cancer is the most common malignancy in women, and also the second leading cause of cancer-related death among female population worldwide.[1] The 5-year patient survival rate drops from 99% to 28% once the breast cancer migrates to distant organs.[2, 3] The key to efficient and ultimately successful therapy of breast cancer is early and precise diagnosis.[4] Direct cancer cell identification, particularly at the nascent phase, is an important strategy for tumour diagnosis since the pathogenesis and development of cancer are closely connected to cell alterations, such as surface marker rearrangement and regulation.[5, 6] As a member of the cell surface receptor tyrosine kinases family,[7] human epidermal growth factor receptor 2 (HER2), which is associated with multiple biological processes including cell differentiation, proliferation, apoptosis, migration, invasion and angiogenesis,[8] is overexpressed in 20%-30% of breast cancers.[9] In comparison with other types of breast cancers, HER2-positive (HER2$^+$) breast cancer has shown enhanced malignancy, increased aggressiveness and poor prognosis, consequently resulting in reduced overall survival.[10, 11] Therefore, the development of new techniques to sensitively and selectively detect HER2$^+$ breast cancer cells is in crucial need for further symptomatic treatment.

Mesoporous silica nanoparticles (MSNs), as one of the most intensively studied inorganic materials, show great potential across a wide spectrum of fields including catalysis, bioseparation, sensing, imaging and environmental science.[12, 13] Among these applications, MSNs are expected to provide an ideal platform for theranostic applications, especially in oncology due to their unique structural features and biological characteristics such as low toxicity, large surface area, high pore volume and cargo-loading capacity, tailorable mesoporous sizes and morphologies, and facile chemical functionalization.[14] Being a well-known trace element in the human body and abundantly distributed throughout nature, silica is categorized as "Generally Recognized As Safe" by the United States Food and Drug Administration (FDA).[15, 16] In addition, silica has also been extensively used commercially in cosmetics and as the excipient in oral drug products, as well as FDA-approved food additives,[16, 17] suggesting the great promise of future clinical translation potentials of silica-based nanoparticles for biomedical applications.[18] Moreover, MSNs are anticipated to greatly extend their bioapplications through the incorporation of other biofunctional nanomaterials.[19-23] In particular, MSNs are attractive enzyme immobilization supports for environmental, catalytic, and biomedical applications.[24]

Development of nanomaterial-based artificial enzyme systems mimicking the catalytic functional natural enzymes attracts increasing attention.[25-28] Among them, the interest in investigating horseradish peroxidase (HRP)-mimicking catalysts extends their application in the fields of biosensing, immunoassays, environmental detection, electrocatalysis, luminescence, and electronics, etc.[29-36] For example, Kim et al. developed the graphene oxide-magnetic-platinum nanohybrids as the HRP-mimicking catalysts for colorimetric cancer detection.[37] As a new type of gold-based nanomaterials that possesses strong photoluminescence

[a] Laboratory of Biomaterials and Translational Medicine, Guangdong Provincial Key Laboratory of Liver Disease, Department of Pediatrics, The Third Affiliated Hospital of Sun Yat-sen University, Guangzhou 510630, China. E-mail: yt2569@cumc.columbia.edu
[b] Department of Biomedical Engineering, Columbia University, New York, NY 10027, United States. E-mail: kam.leong@columbia.edu
[c] Institute for Cancer Genetics, Columbia University Medical Center, New York, NY 10032, United States.
[d] Department of Systems Biology, Columbia University Medical Center, New York, NY 10032, United States.

† Electronic Supplementary Information (ESI) available. See DOI: 10.1039/x0xx00000x

View Article Online
DOI: 10.1039/C8NR08337A

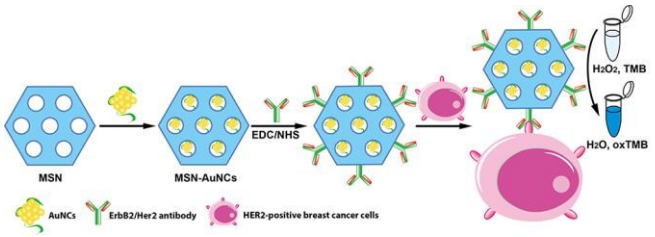

Scheme 1 Schematic illustration of the strategy for HER2$^+$ breast cancer cell sensing by the synergistic amplified colorimetric assay based on MSN-AuNCs-anti-HER2 hybrid.

properties, gold nanoclusters (AuNCs) gather tremendous interest as versatile nanoprobes for luminescent bioimaging and optical material for biosensing.[38-41] Recently, gold nanoclusters show impressive catalytic performance as HRP-mimicking catalysts and serve as promising sensing platforms for biomolecule detections with the merits of tuneable synthesis in low cost, excellent stability, controllable catalytic abilities, as well as ease of storage and implementation.[42-46]

Here, we report on the amplified signal schemes based on the mesoporous silica-gold nanoclusters hybrid (MSN-AuNCs) for efficient HER2$^+$ breast cancer cell detection (Scheme 1). The MSN-AuNCs platform uses the antigen/antibody recognition and the superior catalytic power of AuNCs to realize breast cancer cell targeting and signal amplification. Surface modification of HER2 antibody endows MSN with highly selective sensing of HER2$^+$ breast cancer cells. Meanwhile the high pore volume and large surface area of mesoporous silica make it possible to load a large number of AuNCs in one silica particle, which can efficiently improve the sensitivity of our sensor.

To prove the feasibility of our design, we firstly synthesized the lysozyme-templated gold nanoclusters (AuNCs) and carboxyl modified large pore mesoporous silica nanoparticles (Fig. S1) by following the protocols established by previous works with slight modification.[47-49] Transmission electron microscopy (TEM) (Fig. 1a, 1b) indicated that the AuNCs were monodispersed with a size of about 1.6 nm in diameter (Fig. S2) and the MSNs had spherical structures and large pores with an average diameter around 115 nm (Fig. S3). N_2 adsorption-desorption isotherms of MSN demonstrated their porous structure with a specific surface area of 595 $m^2\ g^{-1}$, and an average pore diameter of 9.85 nm with a narrow pore distribution (Fig. S4), which were consistent with the TEM results. As compared with the TEM observations, dynamic light scattering (DLS) measurements (Table 1) of AuNCs and MSN showed larger size, which can be attributed to the dehydration during the process of TEM specimen preparation and the fact that DLS was sensitive to the interference of large particles.[50, 51] Afterward, the MSN-AuNCs hybrid was prepared by incubating AuNCs with MSNs, based on the electrostatic interaction between AuNCs and MSNs as well as the high loading capacity of mesopores in MSNs. The morphology of the MSN-AuNCs nanohybrid materials was also verified with TEM measurements. As shown in Fig. 1c-d, AuNCs with a narrow diameter distribution were well located in the pores of MSN. DLS measurements suggested that MSN-AuNCs could be well dispersed in the aqueous medium with narrow polydispersity, and the hydrodynamic size of MSN-AuNCs was 158.1 ± 2.5 nm (Table 1). The energy dispersive X-ray spectroscopy (EDS) analysis of the nanohybrid detected the presence of Au signals, verifying the successful loading of AuNCs in MSNs (Fig. S5). EDS served as complementary evidence along with TEM results to support the successful synthesis of MSN-AuNCs hybrids. Afterwards, zeta potential measurements were further utilized to verify the surface property of MSN-AuNCs (Table 1). The reduction in the zeta potential of MSNs after complexation with AuNCs suggested the electrostatic absorption between negatively charged MSNs and positively charged AuNCs. The amount of AuNCs loading in MSNs was measured from the fluorescence decrease of AuNCs in the supernatant and calculated based on an AuNC calibration (Fig. S6).[52, 53] It was estimated that about 202 AuNC molecules were loaded into each MSN. Subsequently, HER2 antibodies were chemically conjugated to MSN-AuNCs (MSN-AuNCs-anti-HER2) by EDC/NHS method. After ligand modification, the hydrodynamic size and surface charge of MSN-AuNCs-anti-HER2 were 167.5 ± 3.2 nm and -25.32 ± 0.54 mV, respectively. The average antibody density was ~232 molecules per MSN, based on the measurement of fluorescence decrease in the supernatant after the reaction (Fig. S7).[52]

MSN-AuNCs-anti-HER2 was active in catalyzing H_2O_2 reduction

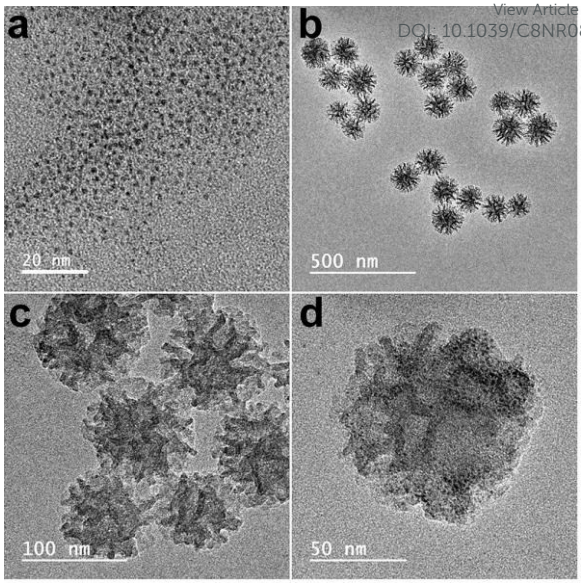

Fig. 1 TEM images of (a) AuNCs, (b) MSN and (c, d) MSN-AuNCs at different magnifications.

Table 1 Main physicochemical characterization for MSN, AuNCs, MSN-AuNCs and MSN-AuNCs-anti-HER2.

Entry	Size (DLS, nm)	Polydispersity Index (PDI)	Zeta potential (mV)
AuNCs	4.5 ± 0.4	0.192	29.90 ± 3.46
MSN	148.5 ± 1.2	0.065	-36.27 ± 0.13
MSN-AuNCs	158.1 ± 2.5	0.118	-26.42 ± 0.07
MSN-AuNCs-anti-HER2	167.5 ± 3.2	0.135	-25.32 ± 0.54

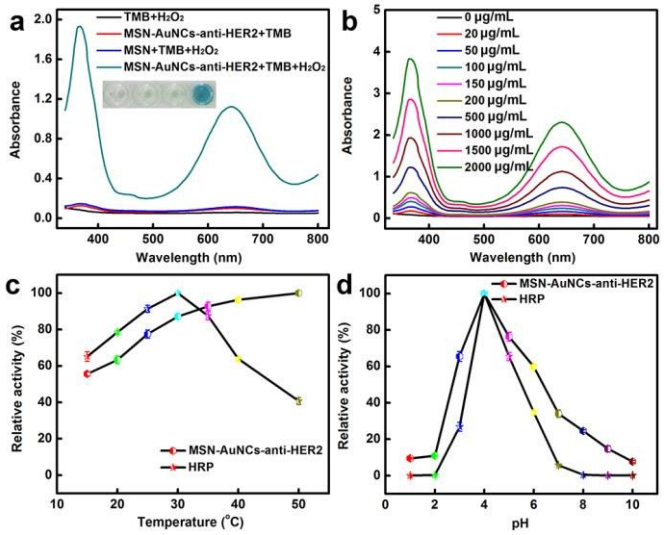

Fig. 2 (a) Absorption spectra and photograph of color reactions of H_2O_2 (black line), MSN-AuNCs-anti-HER2 (red line), H_2O_2 and MSN (blue line), H_2O_2 and MSN-AuNCs-anti-HER2 (green line) after 30 min incubation with TMB. (b) Absorption spectra of H_2O_2-mediated oxidation of TMB catalyzed by MSN-AuNCs-anti-HER2 at different concentrations. (c, d) The temperature (c) and pH (d) dependency of the relative catalytic activity of MSN-AuNCs-anti-HER2. Data are presented as means ± SD (n = 3).

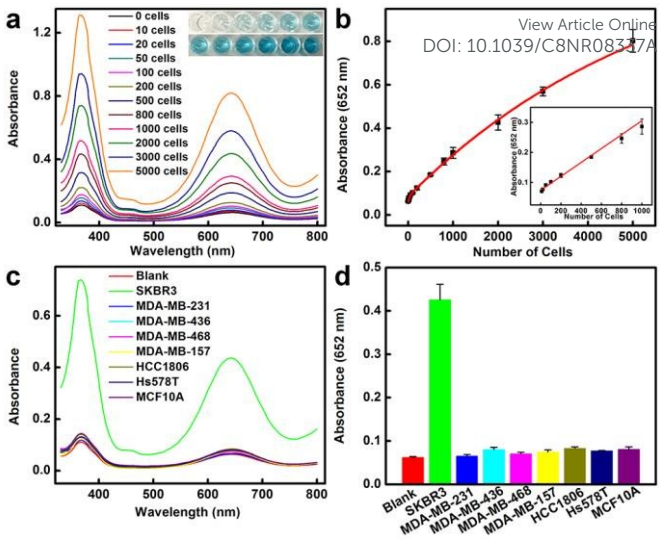

Fig. 3 Discrimination of SKBR3 cells based on MSN-AuNCs-anti-HER2. (a) Photograph and absorption spectra upon sensing of SKBR3 cells. (b) Plot of the absorption values at 652 nm versus different numbers of SKBR3 cells; the inset shows a linear relationship in the range from 10 to 1000 cells. (c) The absorption spectra and (d) absorption intensity at 652 nm of the sensing system in the presence of different types of breast cells. Data are presented as means ± SD (n = 3).

and oxidation of peroxidase substrates 3,3′,5,5′-tetramethylbenzidine (TMB, a common colorimetric agent). As presented in Fig. 2a, MSN-AuNCs-anti-HER2 possessed an intrinsic peroxidase-like property. It was capable of catalyzing H_2O_2 to oxidize TMB, and showed a deep blue color as well as an intense absorption at 652 nm.[54] Since the absorption peak at 652 nm was attributed to the charge-transfer compounds derived from the one-electron oxidation of TMB,[55] we chose absorbance at 652 nm to characterize the catalytic activity of MSN-AuNCs-anti-HER2. In contrast, no obvious absorbance peak and color change could be observed in the absence of MSN-AuNCs-anti-HER2. Moreover, MSN without AuNCs did not produce the oxidation reaction. These results indicated that the catalytic property came from the inherent peroxidase-mimicking activity of AuNCs in MSN-AuNCs-anti-HER2. We then studied the time-dependent absorbance change of the MSN-AuNCs-anti-HER2 at 652 nm to optimize the catalytic efficiency of MSN-AuNCs-anti-HER2 (Fig. S8). The characteristic absorbance gradually increased with the increasing incubation time until reaching a plateau at about 30 min, which was chosen as the incubation time in the following studies. Absorbance spectra for varying concentrations of MSN-AuNCs-anti-HER2 were displayed in Fig. 2b. It can be observed that the TMB oxidation rate was dependent on the MSN-AuNCs-anti-HER2 concentrations. Moreover, similar to other nanozymes, the catalytic ability of MSN-AuNCs-anti-HER2 also relied on H_2O_2 concentration (Fig. S9), temperature (Fig. 2c) and pH (Fig. 2d).

We then applied the MSN-AuNCs-anti-HER2 for construction of a novel and simple colorimetric analysis platform for highly selective and ultrasensitive colorimetric sensing of $HER2^+$ breast cancer cell line SKBR3. The MTT assay indicated that the cellular viability was not affected by MSN-AuNCs-anti-HER2 (Fig. S10). In the absence of the SKBR3 cells, the MSN-AuNCs-anti-HER2 would be removed by the centrifugation and wash steps, showing negligible catalytic activity and color change (Fig. 3a). On the contrary, the introduction of SKBR3 cells would trigger the efficient adsorption of the MSN-AuNCs-anti-HER2 onto target cancer cells for the subsequent colorimetric detection. To calculate the sensitivity of our colorimetric assay, a series of samples containing different amounts of target cells were firstly cultured with MSN-AuNCs-anti-HER2 in PBS and subsequently centrifuged. The cell pellets were gathered and washed thrice with PBS to remove free MSN-AuNCs-anti-HER2. Control tests proved that free MSN-AuNCs-anti-HER2 could be totally removed by centrifugation (Fig. S11). After that, the population of target cancer cells, separated by centrifugation, could be quantified by measuring the color reaction catalyzed by MSN-AuNCs-anti-HER2 when TMB and H_2O_2 were added. Fig. 3a illustrates the absorbance spectra as a function of target cell concentration. The sensitivity of this platform was monitored by absorbance changes of TMB as a function of distinct numbers of SKBR3 cells. The results indicated that along with the increase of cell number, the absorbance at 652 nm progressively enhanced. Additionally, target-concentration-dependent absorption variations were achieved in SKBR3 cells. The constructed nanosensor showed excellent sensitivity allowing for a limit of detection down to 10 cells, with a linear detection range of 10-1000 cells (Fig. 3b). The high sensitivity was attributed to the synergistic effects of extraordinary recognition ability of HER2 antibodies to HER2 receptors on the membranes of SKBR3 breast cancer cells and the excellent catalytic activity of AuNCs (Fig. 3b). Notably, the sensitivity dropped significantly when the assay was done using AuNCs-anti-

View Article Online
DOI: 10.1039/C8NR08377A

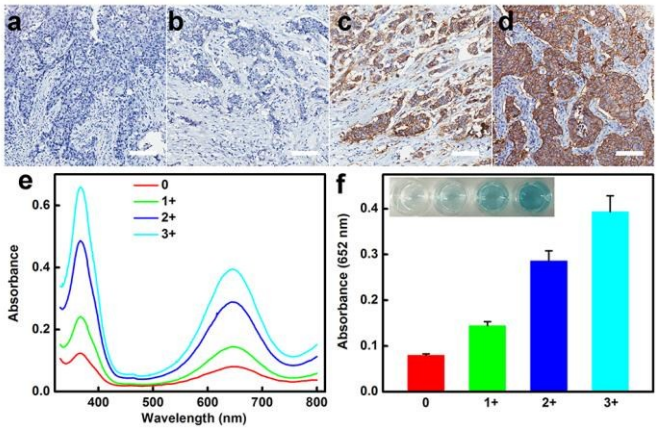

Fig. 4 (a-d) Immunohistochemistry studies of the breast cancer tissue array (HER2 scores: 3+ (d)/2+ (c)/1+ (b)/0 (a)). The bar represents 100 µm. (e-f) The applicability of the developed method for real sample HER2$^+$ breast cancer tissue monitoring. (e) Absorption spectra responses and (f) the evolution of the absorption at 652 nm with the increment of HER2 scores. Data are presented as means ± SD (n = 3).

HER2 without the MSNs, demonstrating the MSN-assisted enzyme enrichment was essential for achieving low detection limit for target cell detection (Fig. S12). In addition, since cancer cells usually present the low-density target surface marker for recognition at early stages of cancer progression, multivalent antibody binding of MSN-AuNCs-anti-HER2 is considered to be advantageous for early cancer diagnosis.[56, 57]

To further verify the selectivity of our colorimetric method, assays were conducted on eight distinctive human breast cell types, involving HER2$^+$ SKBR3 breast cancer cell, six types of triple-negative breast cancer cells (HCC1806, MDA-MB-231, MDA-MB-468, Hs578T, MDA-MB-436 and MDA-MB-157) and the non-neoplastic, fibrocystic breast cell MCF10A (Fig. 3c, d). After 1.5 h culture and reaction, the absorbance signals derived from the MSN-AuNCs-anti-HER2 oxidation of TMB for SKBR3 cells increased significantly compared with other types of breast cells and the blank, which was ascribed to the high affinity of MSN-AuNCs-anti-HER2 to HER2 receptors and the high HER2 receptor expression on SKBR3 cells. This contrasting difference demonstrates that the proposed approach is highly specific and sensitive for colorimetric cell detection.

Next we evaluated if the combination of excellent specificity and high sensitivity of this colorimetric sensor could be duplicated in measuring breast cancer tissues with different HER2 expression levels (Fig. 4). The immunohistochemistry (IHC) test (Fig. 4a-d) gave a score ranging from 0–3+, which represented the amount of HER2 receptors on the cell surfaces. A score of 0 or 1+ indicated that the breast cancer was HER2 negative. A score of 2+ was weakly positive, and 3+ indicated the breast cancer was strongly HER2 positive, with ≥10% of tumor cells with complete membrane staining.[7, 58] In comparison with specimens of HER2-negative tissues, the HER2$^+$ cancer tissue samples exhibited greatly enhanced absorbances, suggesting more HER2$^+$ tumor cells in these tissues (Fig. 4e-f). The absorbance signals increased along with the rising HER2 IHC scores, revealing that the MSN-AuNCs-anti-HER2-based biosensor showed great practicality for efficient analysis of HER2$^+$ breast cancer tissue, and hereafter might present a promising potential for clinical diagnosis.

Conclusions

In summary, taking advantage of the peroxidase mimicking activity of AuNCs, we report a novel colorimetric assay based on the HER2 antibody attached to a MSN-AuNCs hybrid platform for HER2$^+$ breast cancer cell detection. Leveraging on the specificity of the HER2 antibody and the catalytic capability of AuNCs, we show a biosensor design that is sensitive, selective, economic and simple in operation. The monitoring of HER2$^+$ breast cancer cells from tumor tissue demonstrates its potential application in clinical diagnosis. This approach can be easily extended to other cells by simply changing the recognition ligand for a variety of applications involving point-of-care cancer diagnostics, bioanalysis and bionanotechnology.

Conflicts of interest

There are no conflicts to declare.

Acknowledgements

Funding support from NIH (GM110494 and R21 HL140275), Guangdong Innovative and Entrepreneurial Research Team Program (2013S086), Global Research Laboratory Program (Korean NSF GRL; 2015032163) and National Natural Science Foundation of China (81470219) is acknowledged.

Notes and references

1. M. Li, Z. Tang, D. Zhang, H. Sun, H. Liu, Y. Zhang, Y. Zhang and X. Chen, *Biomaterials*, 2015, **51**, 161-172.
2. Y. Tao and D. T. Auguste, *Biosens. Bioelectron.*, 2016, **81**, 431-437.
3. R. L. Siegel, K. D. Miller and A. Jemal, *Ca-Cancer J. Clin.*, 2018, **68**, 7-30.
4. P. Wu, Y. Gao, H. Zhang and C. Cai, *Anal. Chem.*, 2012, **84**, 7692-7699.
5. W. Lu, A. K. Singh, S. A. Khan, D. Senapati, H. Yu and P. C. Ray, *J. Am. Chem. Soc.*, 2010, **132**, 18103-18114.
6. R. O. P. Draga, M. C. M. Grimbergen, P. L. M. Vijverberg, C. F. P. v. Swol, T. G. N. Jonges, J. A. Kummer and J. L. H. Ruud Bosch, *Anal. Chem.*, 2010, **82**, 5993-5999.
7. B. P. Joshi, J. Zhou, A. Pant, X. Duan, Q. Zhou, R. Kuick, S. R. Owens, H. Appelman and T. D. Wang, *Bioconjugate Chem.*, 2016, **27**, 481-494.
8. T. Y. Rakovich, O. K. Mahfoud, B. M. Mohamed, A. Prina-Mello, K. Crosbie-Staunton, T. Van Den Broeck, L. De Kimpe, A. Sukhanova, D. Baty, A. Rakovich, S. A. Maier, F. Alves, F. Nauwelaers, I. Nabiev, P. Chames and Y. Volkov, *ACS Nano*, 2014, **8**, 5682-5695.

9. E. A. Rakha, S. E. Pinder, J. M. S. Bartlett, M. Ibrahim, J. Starczynski, P. J. Carder, E. Provenzano, A. Hanby, S. Hales, A. H. S. Lee and I. O. Ellis, *J. Clin. Pathol.*, 2015, **68**, 93-99.
10. M. J. van de Vijver, Y. D. He, L. J. van 't Veer, H. Dai, A. A. M. Hart, D. W. Voskuil, G. J. Schreiber, J. L. Peterse, C. Roberts, M. J. Marton, M. Parrish, D. Atsma, A. Witteveen, A. Glas, L. Delahaye, T. van der Velde, H. Bartelink, S. Rodenhuis, E. T. Rutgers, S. H. Friend and R. Bernards, *N. Engl. J. Med.*, 2002, **347**, 1999-2009.
11. C. Chen, S.-R. Sun, Y.-P. Gong, C.-B. Qi, C.-W. Peng, X.-Q. Yang, S.-P. Liu, J. Peng, S. Zhu, M.-B. Hu, D.-W. Pang and Y. Li, *Biomaterials*, 2011, **32**, 7592-7599.
12. J. Shi, *Chem. Rev.*, 2013, **113**, 2139-2181.
13. Z. Li, J. C. Barnes, A. Bosoy, J. F. Stoddart and J. I. Zink, *Chem. Soc. Rev.*, 2012, **41**, 2590-2605.
14. Y. Chen, H. Chen and J. Shi, *Adv. Mater.*, 2013, **25**, 3144-3176.
15. D. Ni, D. Jiang, E. B. Ehlerding, P. Huang and W. Cai, *Acc. Chem. Res.*, 2018, **51**, 778-788.
16. J. Kim, W. A. Li, Y. Choi, S. A. Lewin, C. S. Verbeke, G. Dranoff and D. J. Mooney, *Nat. Biotechnol.*, 2015, **33**, 64-72.
17. F. Tang, L. Li and D. Chen, *Adv. Mater.*, 2012, **24**, 1504-1534.
18. Y. Zhang, B. Y. W. Hsu, C. Ren, X. Li and J. Wang, *Chem. Soc. Rev.*, 2015, **44**, 315-335.
19. H. Mekaru, J. Lu and F. Tamanoi, *Adv. Drug Delivery Rev.*, 2015, **95**, 40-49.
20. J. Kim, H. R. Cho, H. Jeon, D. Kim, C. Song, N. Lee, S. H. Choi and T. Hyeon, *J. Am. Chem. Soc.*, 2017, **139**, 10992-10995.
21. D. Tarn, C. E. Ashley, M. Xue, E. C. Carnes, J. I. Zink and C. J. Brinker, *Acc. Chem. Res.*, 2013, **46**, 792-801.
22. Z. Liu, Y. Li, W. Li, C. Xiao, D. Liu, C. Dong, M. Zhang, E. Makila, M. Kemell, J. Salonen, J. T. Hirvonen, H. Zhang, D. Zhou, X. Deng and H. A. Santos, *Adv. Mater.*, 2018, **30**, e1703393.
23. W. Han, A. Chilkoti and G. P. Lopez, *Nanoscale*, 2017, **9**, 6178-6186.
24. Q. Yue, J. Li, W. Luo, Y. Zhang, A. A. Elzatahry, X. Wang, C. Wang, W. Li, X. Cheng, A. Alghamdi, A. M. Abdullah, Y. Deng and D. Zhao, *J. Am. Chem. Soc.*, 2015, **137**, 13282-13289.
25. M. Raynal, P. Ballester, A. Vidal-Ferran and P. W. N. M. van Leeuwen, *Chem. Soc. Rev.*, 2014, **43**, 1734-1787.
26. H. Wei and E. Wang, *Chem. Soc. Rev.*, 2013, **42**, 6060-6093.
27. Y. Lin, J. Ren and X. Qu, *Acc. Chem. Res.*, 2014, **47**, 1097-1105.
28. H. Aldewachi, T. Chalati, M. N. Woodroofe, N. Bricklebank, B. Sharrack and P. Gardiner, *Nanoscale*, 2018, **10**, 18-33.
29. Z. Tian, J. Li, Z. Zhang, W. Gao, X. Zhou and Y. Qu, *Biomaterials*, 2015, **59**, 116-124.
30. S. Wang, W. Deng, L. Yang, Y. Tan, Q. Xie and S. Yao, *ACS Appl. Mater. Interfaces*, 2017, **9**, 24440-24445.
31. N. Lu, M. Zhang, L. Ding, J. Zheng, C. Zeng, Y. Wen, G. Liu, A. Aldalbahi, J. Shi, S. Song, X. Zuo and L. Wang, *Nanoscale*, 2017, **9**, 4508-4515.
32. X. Wang, W. Cao, L. Qin, T. Lin, W. Chen, S. Lin, J. Yao, X. Zhao, M. Zhou, C. Hang and H. Wei, *Theranostics*, 2017, **7**, 2277-2286.
33. P. Gopinath, V. Ramalingam and R. Breslow, *Proc. Natl. Acad. Sci. U. S. A.*, 2015, **112**, 12011-12014.
34. K. Yang, G. Yang, L. Chen, L. Cheng, L. Wang, C. Ge and Z. Liu, *Biomaterials*, 2015, **38**, 1-9.
35. M. Vázquez-González, W.-C. Liao, R. Cazelles, S. Wang, X. Yu, V. Gutkin and I. Willner, *ACS Nano*, 2017, **11**, 3247-3253.
36. T. Xue, B. Peng, M. Xue, X. Zhong, C.-Y. Chiu, S. Yang, Y. Qu, L. Ruan, S. Jiang, S. Dubin, R. B. Kaner, J. I. Zink, M. E. Meyerhoff, X. Duan and Y. Huang, *Nat. Commun.*, 2014, **5**, 3200.
37. M. I. Kim, M. S. Kim, M. A. Woo, Y. Ye, K. S. Kang, J. Lee and H. G. Park, *Nanoscale*, 2014, **6**, 1529-1536.
38. S. H. Yau, O. Varnavski and T. Goodson, 3rd, *Acc. Chem. Res.*, 2013, **46**, 1506-1516.
39. Y. Lei, L. Tang, Y. Xie, Y. Xianyu, L. Zhang, P. Wang, Y. Hamada, K. Jiang, W. Zheng and X. Jiang, *Nat. Commun.*, 2017, **8**, 15130.
40. R. Vankayala, C.-L. Kuo, K. Nuthalapati, C.-S. Chiang and K. C. Hwang, *Adv. Funct. Mater.*, 2015, **25**, 5934-5945.
41. Y. Tao, M. Li, J. Ren and X. Qu, *Chem. Soc. Rev.*, 2015, **44**, 8636-8663.
42. Y. Tao, Y. Lin, J. Ren and X. Qu, *Biosens. Bioelectron.*, 2013, **42**, 41-46.
43. G.-L. Wang, L.-Y. Jin, Y.-M. Dong, X.-M. Wu and Z.-J. Li, *Biosens. Bioelectron.*, 2015, **64**, 523-529.
44. Y. Tao, Y. H. Lin, Z. Z. Huang, J. S. Ren and X. G. Qu, *Adv. Mater.*, 2013, **25**, 2594-2599.
45. S. Das, A. Goswami, M. Hesari, J. F. Al-Sharab, E. Mikmeková, F. Maran and T. Asefa, *Small*, 2014, **10**, 1473-1478.
46. Y. Tao, M. Li, B. Kim and D. T. Auguste, *Theranostics*, 2017, **7**, 899–911.
47. Y. H. Lin and W. L. Tseng, *Anal. Chem.*, 2010, **82**, 9194-9200.
48. H. Wei, Z. D. Wang, L. M. Yang, S. L. Tian, C. J. Hou and Y. Lu, *Analyst*, 2010, **135**, 1406-1410.
49. K. Zhang, L.-L. Xu, J.-G. Jiang, N. Calin, K.-F. Lam, S.-J. Zhang, H.-H. Wu, G.-D. Wu, B. Albela, L. Bonneviot and P. Wu, *J. Am. Chem. Soc.*, 2013, **135**, 2427-2430.
50. Y. Tao, E. Ju, J. Ren and X. Qu, *Adv Mater*, 2015, **27**, 1097-1104.
51. M. Li, Z. Tang, S. Lv, W. Song, H. Hong, X. Jing, Y. Zhang and X. Chen, *Biomaterials*, 2014, **35**, 3851-3864.
52. L. Pan, Q. He, J. Liu, Y. Chen, M. Ma, L. Zhang and J. Shi, *J. Am. Chem. Soc.*, 2012, **134**, 5722-5725.
53. Y. Tao, E. Ju, Z. Liu, K. Dong, J. Ren and X. Qu, *Biomaterials*, 2014, **35**, 6646-6656.
54. L. A. Marquez and H. B. Dunford, *Biochemistry*, 1997, **36**, 9349-9355.
55. P. D. Josephy, T. Eling and R. P. Mason, *J. Biol. Chem.*, 1982, **257**, 3669-3675.
56. W. Lu, S. R. Arumugam, D. Senapati, A. K. Singh, T. Arbneshi, S. A. Khan, H. Yu and P. C. Ray, *ACS Nano*, 2010, **4**, 1739-1749.
57. H.-Z. Chen, S.-Y. Tsai and G. Leone, *Nat. Rev. Cancer*, 2009, **9**, 785.
58. A. Cayre, F. Mishellany, N. Lagarde and F. Penault-Llorca, *Breast Cancer Res.*, 2007, **9**, R64.

View Article Online
DOI: 10.1039/C8NR08337A

TOC

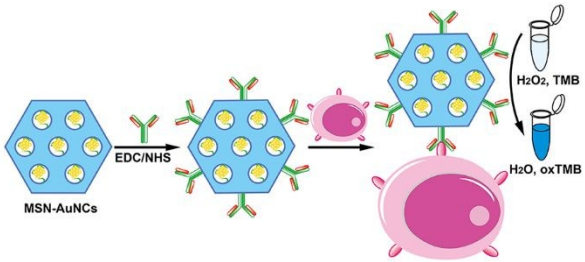

Breast cancer detection: Biosensor based on HER2 antibodies attached to MSN-AuNCs hybrids, is sensitive, selective, economic and simple in operation.